Quantitative characterization of metastatic disease in the spine. Part II. Histogram-based analyses

Cari Whyne,[a] Michael Hardisty, Florence Wu, and Tomas Skrinskas
Orthopaedic Biomechanics Laboratory, Sunnybrook Health Sciences Centre, 2075 Bayview Avenue, Room UB-19, Toronto, Ontario M4N 3M5, Canada

Mark Clemons
Breast Medical Oncology, Princess Margaret Hospital, 610 University Avenue, Room 5-205, Toronto, Ontario M5G 2M9, Canada

Lyle Gordon
Orthopaedic Biomechanics Laboratory, Sunnybrook Health Sciences Centre, 2075 Bayview Avenue, Room UB-19, Toronto, Ontario M4N 3M5, Canada

Parminder S. Basran
Department of Medical Physics, Toronto Sunnybrook Regional Cancer Centre, 2075 Bayview Avenue, Room TG-217, Toronto, Ontario M4N 3M5, Canada

(Received 30 August 2006; revised 19 June 2007; accepted for publication 19 June 2007; published 24 July 2007)

Radiological imaging is essential to the appropriate management of patients with bone metastasis; however, there have been no widely accepted guidelines as to the optimal method for quantifying the potential impact of skeletal lesions or to evaluate response to treatment. The current inability to rapidly quantify the response of bone metastases excludes patients with cancer and bone disease from participating in clinical trials of many new treatments as these studies frequently require patients with so-called measurable disease. Computed tomography (CT) can provide excellent skeletal detail with a sensitivity for the diagnosis of bone metastases. The purpose of this study was to establish an objective method to quantitatively characterize disease in the bony spine using CT-based segmentations. It was hypothesized that histogram analysis of CT vertebral density distributions would enable standardized segmentation of tumor tissue and consequently allow quantification of disease in the metastatic spine. Thirty two healthy vertebral CT scans were first studied to establish a baseline characterization. The histograms of the trabecular centrums were found to be Gaussian distributions (average root-mean-square difference=30 voxel counts), as expected for a uniform material. Intrapatient vertebral level similarity was also observed as the means were not significantly different ($p>0.8$). Thus, a patient-specific healthy vertebral body histogram is able to characterize healthy trabecular bone throughout that individual's thoracolumbar spine. Eleven metastatically involved vertebrae were analyzed to determine the characteristics of the lytic and blastic bone voxels relative to the healthy bone. Lytic and blastic tumors were segmented as connected areas with voxel intensities between specified thresholds. The tested thresholds were $\mu-1.0\sigma$, $\mu-1.5\sigma$, and $\mu-2.0\sigma$, for lytic and $\mu+2.0\sigma$, $\mu+3.0\sigma$, and $\mu+3.5\sigma$ for blastic tissue where μ and σ were taken from the Gaussian characterization of a healthy level within the same patient. The ideal lytic and blastic segmentation thresholds were determined to be $\mu-\sigma$ and $\mu+2\sigma$, respectively. Using the optimized thresholds to segment tumor tissue, a quantitative characterization of disease is possible to calculate tumor volumes, disease severity, and temporal progression or treatment effect. Our proposed histogram-based method for characterizing spinal metastases shows great potential in extending the quantitative capacity of CT-based radiographic evaluations. © *2007 American Association of Physicists in Medicine*. [DOI: 10.1118/1.2756939]

Key words: spine, vertebrae, image analysis, image segmentation, breast cancer

I. INTRODUCTION

Bone is one of the most common sites to which cancer metastasizes. For a number of reasons, including blood flow, the spine is a frequent site of metastatic spread. Indeed, spinal metastases originate from a wide range of tumor types such as prostate (90%), breast (75%), lung (45%), and renal (30%) cancer.[1] The complications of bone metastasis include bone pain, pathologic fractures, hypercalcemia, and spinal cord compression.[2,3] Reducing the skeletal complications can significantly improve the quality of life for patients with metastatic disease.[4–9]

Radiological imaging is essential to the appropriate management of patients with bone metastasis; however, there have been no widely accepted guidelines as to the optimal method for quantifying the potential impact of skeletal lesions or to evaluate response to treatment. The criteria developed by the International Union Against Cancer (UICC)[10,11]

and the WHO[12] to assess bone tumor response using plain radiography (XR) and skeletal scintigraphy (SS) frequently do not meet the needs of oncologists in clinical practice.[13] The Response Evaluation Criteria in Solid Tumors (RECIST)[14] group goes as far as to consider bone disease and its progression or response to treatment to be "nonmeasurable." This situation results in heterogeneity in assessments of bone metastasis by oncologists. Indeed, the current inability to rapidly quantify the response of bone metastases excludes patients with cancer and bone disease from participating in clinical trials of many new treatments as these studies frequently require patients with so-called measurable disease.[13]

Even when standard protocols for clinical assessment and follow-up of spinal metastatic disease are conducted through conventional XR and SS, the sensitivity and specificity of assessments using these techniques are not sufficient to give adequate quantitative measures of tumor involvement, progression, or response to treatment. Using XR, 30% to 75% of normal bone mineral content must be lost before osteolytic lesions in the lumbar vertebrae become apparent due to limited contrast in trabecular bone.[15–18] As such, XR is not very sensitive (44% to 50%) for detecting or tracking bone metastasis.[15,17,19–22] Tumor dimensions and bone destruction are difficult to measure on plain radiographs, and response to therapy is often not assessed by decreases in the radius or diameter of the radiographic lesion, but rather by the reappearance of new bone or sclerotic changes, which are very difficult to quantify. Similarly, false-positive and false-negative findings characteristic of SS impede the assessment of bone tumor response due to its relative lack of specificity. Increases in bone metabolic rates can be caused by noncancer related conditions such as fracture, arthritis, or infection.[17,21,23–30] Other ambiguous appearances on SS are "flares" resulting from the reparative process that may occur in the first 3 months after treatment and "cold spots" reflecting a reduction in isotope uptake, which can occur in rapidly progressing disease.[27,31,32]

Computed tomography (CT) can provide excellent skeletal detail, with a sensitivity for the diagnosis of bone metastases ranging from 71% to 100%.[23,33,34] CT is also better than XR and SS for depicting lesions in the spine.[35,36] In evaluating clinical treatments for spinal metastases, however, the use of CT has been limited for the most part to qualitative assessments or quantitative assessments of two-dimensional (2D) slices.[37] A reliable diagnosis of tumor volumes and progression through serial CT scans can be hindered by the subjective and inconsistent nature of visually contouring regions of interest (ROIs) from stacks of 2D images viewed at nonstandardized grayscale mappings; greater sensitivity to disease progression is possible with 3D analyses of the entire lesion. Attempts at quantification that simply calculate mean densities over a ROI also fail to elucidate the true severity and spatial distribution of spinal metastases, particularly in mixed lesions.

Histogram analyses of CT images have been used to differentiate metastatic and nonmetastatic tissue in multiple anatomic sites (lung, adrenal gland).[38,39] Histogram based techniques are much more sensitive than hard threshold values to distinguish metastatic from normal tissue.[38] Evaluations based on the distribution of tissue attenuation can provide more sensitivity than is available from overall mean attenuation data.[38]

The purpose of this study was to establish an objective method to quantitatively characterize the extent of metastatic disease in the bony spine using CT segmentation. It was hypothesized that histogram analysis of the vertebral centrum intensity distributions of CT scans would enable standardized segmentation of tumor tissue and consequently allow quantification of disease in the metastatic spine. As a first step, we characterized the bone density distribution in healthy vertebrae. We were then able to segment metastatic tissue from the established healthy baseline to quantify disease involvement. As a precursor to this analysis, Part 1[40] of this study describes the methodology for segmentation of the trabecular centrum that is referenced in the formulation of this work.

II. CHARACTERIZING HEALTHY VERTEBRAE

The vertebral bodies encompass 80% of spinal metastatic spread. The propensity of spread within the vertebral body may be due to the presence of vasculature, which allows tumor cells to easily seed in this region. As well this region has a greater volumetric size than the posterior elements. Thus the ROI for analysis in this study was chosen as the trabecular centrum of the vertebral body (VB). In order to characterize metastatic VBs, we first established the uniformity of the trabecular centrums of healthy VBs.

A. Methods

Thirty-two healthy vertebrae (sampled from seven patients and spanning vertebral levels T4 to L5) were studied. All healthy levels from each patient were used, stated as such in the imaging reports either explicitly or from lack of mention in describing other pathologies and confirmed through visual inspection. A research protocol standardized serial patient thoracolumbar spinal CT scans from a GE Lightspeed Plus CT Scanner, Fairfield, CT, at 120 kVp, 1.25 mm slice interval, and 2.5 mm slice thickness. Standard reconstructions, featuring enhanced contrast resolution, were found to be optimal for differentiating small density differences between metastatic tissue and normal bone. The variation in reconstructed diameters (DFOV 18 to 24 cm) was compensated for by down-sampling all scans to a common pixel spacing of $0.468/0.468\ \text{mm}^2$, using a Lanczos resampling algorithm. The resampling maintained a voxel intensity distribution concurrency of 98% between scans (Amira 3.1.1, TGS, Berlin) as determined through cadaveric phantom studies. The voxel intensity distribution histograms of the ROIs [histogram plots of voxel counts over tissue density in Hounsfield units (HU)] were plotted for all healthy levels (Fig. 1). Gaussian regression curves,

TABLE I. Summary of Gaussian fits to healthy vertebral centrums. μ and σ denote parameters obtained by the curve fitting. RMSD is the root mean square difference of the fit and the actual distribution of intensities. STD denotes the standard deviation. The standard deviations of μ are much lower within patients than between patients.

Scan	N	$\mu \pm$STD	$\sigma \pm$STD	RMSD$\pm$STD	Derived blastic threshold	Derived lytic threshold
1	5	272.7±18.1	68.7±9.5	33.9±21.6	410.2	204.0
2	2	167.9±19	59.4±1.9	63.0±34.2	286.8	108.4
3	3	182.6±11.2	55.6±2.6	32.9±24.2	293.8	126.9
4	4	199.2±7.3	53.7±3.9	32.0±26.1	306.6	145.5
5	6	268±13.1	53.4±7.3	29.2±16.2	374.9	214.6
6	2	153.1±9.4	42.8±6.4	28.8±8.1	238.6	110.4
7	2	129.6±6.8	69.2±3.6	25.8±1.2	268.0	60.5
8	3	190±35.1	63.5±5.8	37.2±16.6	321.1	124.4
9	5	198.7±3.9	58.3±4.7	27.6±13.4	315.3	140.4
Thoracic	20	222.4±48.2	56.5±8.0	21.2±9.4	335.4	168.0
Lumbar	12	194.4±43.7	62.3±13.3	52.6±21.8	318.9	132.1
Total	32	211.9±48.5	58.6±10.7	33.0±21.5	329.2	153.3

$$f_h(x) = A_h e^{[-(x-\mu)^2/2\sigma^2]}, \quad (1)$$

were fit to the histograms, where μ is the mean, σ is the standard deviation, and A_h is a term that scales segmented healthy ROI volumes. A least-squares curve-fitting of the Gaussian was performed using Matlab (Mathworks, Natick). The accuracy of the regression curves was measured by their root-mean-square difference (RMSD) given in voxel counts. Intrapatient vertebral histograms were compared using one-way repeated measures ANOVA ($p<0.05$) and calculation of the standard error of the intrapatient means.

B. Results

The histograms of the trabecular centrums of the 32 healthy vertebrae were found to be Gaussian distributions (average RMSD=30±18 voxel counts), as expected for a uniform material (Fig. 1). The Gaussian μ ranged from 120 to 290 HU within our tested samples of healthy ROIs. The differences may be due to intrapatient bone variability and/or scanning parameters. However, the histogram data sets were not significantly different ($p>0.8$) across intrapatient vertebral levels T5–L5 (Fig. 2). Furthermore, intrapatient means had standard errors ranging from 7 to 22 HU (Table I). Thus, a patient-specific healthy ROI histogram is able to characterize healthy trabecular bone throughout that individual's thoracolumbar spine.

III. CHARACTERIZING METASTATICALLY INVOLVED VERTEBRAE

A qualitative observation of the histograms for metastatic vertebrae reveals a distinct peak of low intensity voxels representing lytic tumors and a broad thick tail of high-intensity voxels for blastic tissue (Fig. 3). The proposed method for segmenting these regions aims to take advantage of their distinct patterns and deviations from a healthy Gaussian distribution.

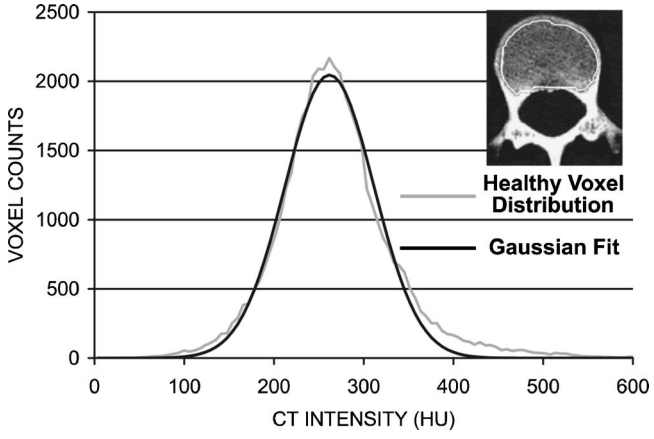

FIG. 1. Voxel intensity histogram of a healthy vertebra. The healthy vertebral body trabecular centrum displays a CT intensity distribution of a uniform material. A Gaussian curve closely characterizes the trabecular ROI.

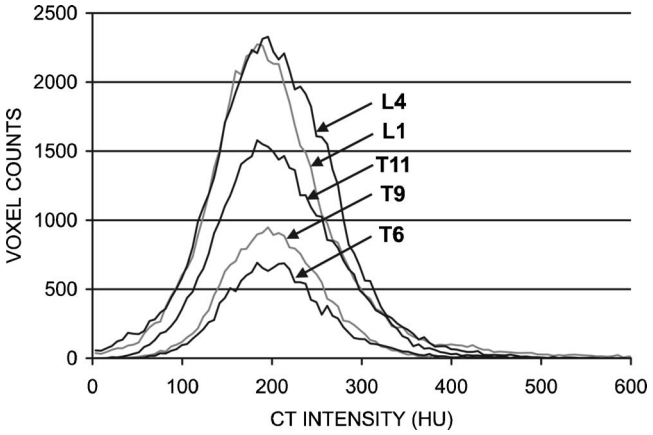

FIG. 2. Intrapatient healthy intensity histograms. Intrapatient healthy vertebral levels demonstrated similar histogram means and standard deviations. Representative distributions are shown for various levels in a single patient where the means range from 193 to 198 HU.

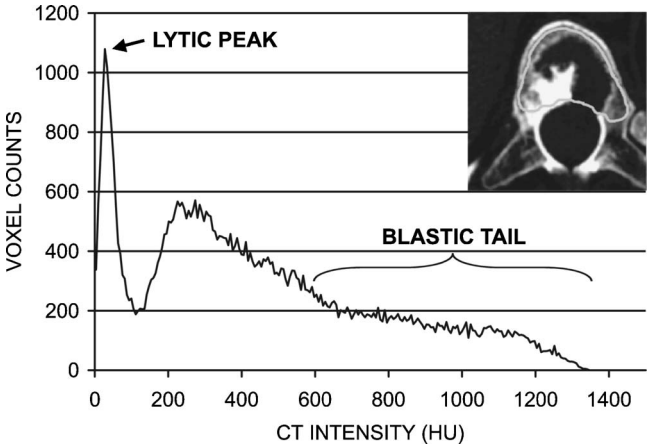

FIG. 3. Histogram of a metastatic vertebral body. Metastatically involved vertebrae no longer have Gaussian distributions. Lytic tumors present a distinct peak of low-intensity (dark) voxels while blastic tissue (bright) results in a tail of high-intensity voxels.

Intrapatient healthy vertebral levels maintained the same mean and standard deviation of bone intensity for the ROIs. We can take advantage of this consistency between levels to analyze a metastatically involved vertebra. It was hypothesized that the lytic and blastic voxels are respectively below and above thresholds that are functions of the healthy mean and standard deviation.

A. Methods

CT scans using the aforementioned parameters and reconstructions were obtained for 12 metastatically involved vertebrae (sampled from ten patients, five thoracic, and seven lumbar) with distinct foci of disease. Lytic and blastic tumors were segmented using the magic wand tool in Amira. The magic wand tool segments voxels that are connected to a seed that fall within a previously provided intensity range. The seeded locations must be placed within the tumors, but the segmentations are insensitive to the exact location within the tumor. In our analysis, clearly distinct lytic and blastic focal lesions were seeded by the user. The tested intensity ranges for lytic tissue were all voxels falling below thresholds of $\mu-1.0\sigma$, $\mu-1.5\sigma$, and $\mu-2.0\sigma$, and for blastic tissue, voxels above thresholds of $\mu+2.0\sigma$, $\mu+3.0\sigma$, and $\mu+3.5\sigma$ where μ and σ are taken from the Gaussian characterization of a healthy level within the same patient. The healthy level was chosen to be as close as possible to the level of interest, although, as determined in Sec. II B, a ROI from any healthy vertebral level can provide adequate mean and standard deviation values to be used in the analysis of the metastatic level.

The segmented metastatically involved regions were then removed from the distributions of the diseased ROIs. Upon fitting Gaussians to the remaining healthy voxels, the ideal segmentation thresholds were defined as those that best restored the Gaussian uniformity of the remaining voxels. Manual segmentations of metastatic disease in the spine do not yield a gold standard for comparison, particularly when diffuse disease is present. Thus, a comparison to manually delineated disease is not considered as a measure of the ability of our algorithm. Instead, based on the consistent Gaussian distribution found throughout healthy vertebral levels of each individual's spine, the impact of disease can be assessed, as a perfectly segmented lesion removed from the ROI would leave behind only voxels representing the healthy level Gaussian distribution. RMSD was used as a measure of Gaussian fit to the remaining healthy voxels. The segmentations that best restored normal histograms were then compared to those conducted by an orthopaedic spine surgeon (the co-director of the Bone Metastases Clinic at our institution) as a further validation of the approach.

B. Results

By studying the uniformity of the remaining healthy voxels, ideal lytic and blastic segmentation thresholds were determined to be $\mu-\sigma$ and $\mu+2\sigma$, respectively (Fig. 4). While the histograms of metastatic VBs were non-Gaussian (RMSD of 108±64 voxels), subtracting from them the tumorous regions was found to improve the Gaussian nature of the distributions (RMSD of 56±39 voxels). The histograms approached Gaussian distributions following the removal of tumor voxels with an average reduction in RMSD of 51 voxels. A qualitative observation supported the ideal thresholds as defined by the RMSD of the remaining healthy voxels. The segmentations compared well to segmentations done by an expert user. (Volumetric concurrency: Well-defined lesions ($n=6$): 88.9%+5.7%; poorly defined lesions ($n=6$): 74.1%+5.0%). The distinct lesions analyzed in this study separated into two groups of equal size. The first group had well-defined distinct lesions, while the second group had distinct lesions that were not well defined consisting of a mixture of multiple distinct foci and diffuse disease. The lower volumetric concurrency in the poorly defined vertebrae can be attributed to the greater difficulty of the expert user in defining the boundaries of the lesions. The tumorous vertebrae examined ranged from predominately blastic to predominantly lytic disease. The vertebrae ranged from having 21% lytic disease to having 96% of the vertebrae taken up by blastic tissue. As a result, the mean of the vertebral intensities prior to removal of tumorous tissue ranged from 211 to 935 HU.

C. Tumor quantification

Using the optimized thresholds to segment tumor tissue, a quantitative characterization of disease was possible to determine:

1. Segmentations for diffuse tumors without distinct foci where our parameters are applied to the ROIs without seeding, effectively thresholding the volume for tumor tissue. This automated technique is without user bias and ensures a standard for temporal changes in tumor volume.

2. The volume (%, cm^3) of lytic and/or blastic tissue obtained from the respective segmentations.

3. The severity of the pathologic involvement from the total histogram range (Fig. 5).

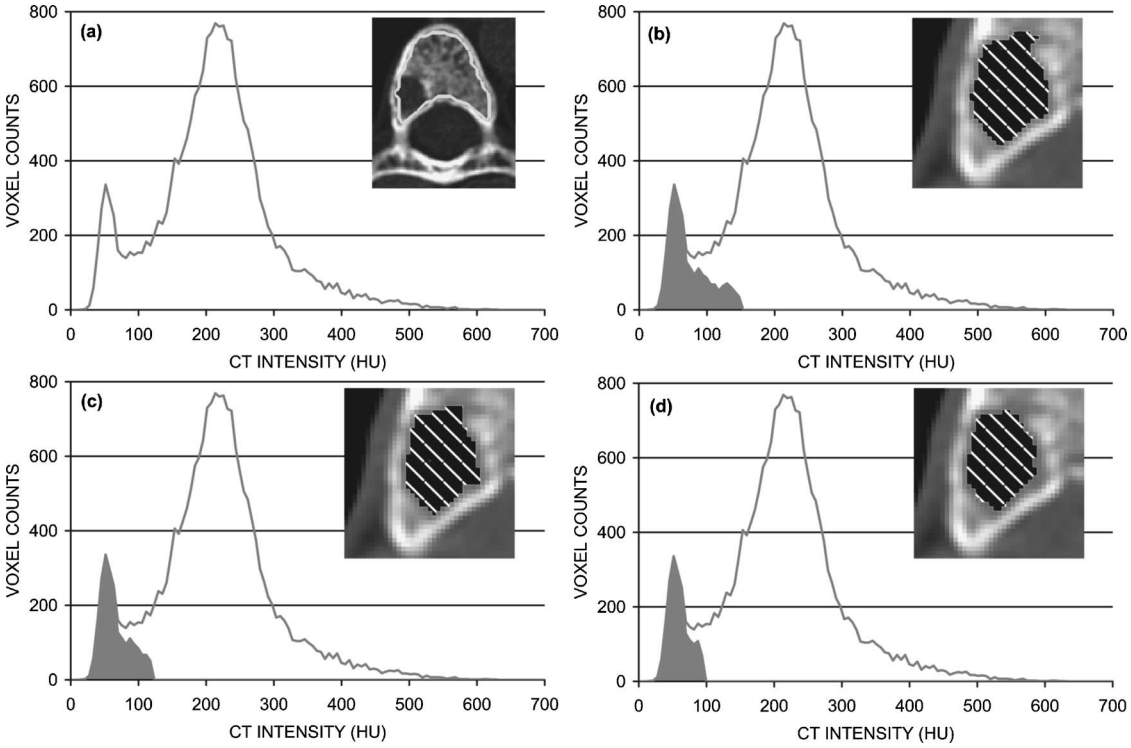

FIG. 4. Lytic tumor segmentation threshold. Histograms are depicted for (a) representative lytic lesion and the three tested segmentation thresholds of (b) $\mu-1.0\sigma$, (c) $\mu-1.5\sigma$, and (d) $\mu-2.0\sigma$. Sample CT slices and shaded segmentations are shown.

4. The progression of tumors over time or treatment effect through the differences between initial and sequential or posttreatment histograms (Fig. 6).

IV. DISCUSSION

Using a histogram analysis of density distributions in CT scans of metastatically involved vertebrae, an objective method was established to quantitatively characterize the extent and distribution of disease in the bony spine. The consistency of the Gaussian distributions of the trabecular centrum of healthy vertebral levels within individual patients yields intrapatient specific baselines upon which lytic and blastic activity can be quantified. By using thresholds relative to the means and standard deviations of healthy vertebra interpatient variability in bone quality can be accounted for.

The proposed lytic and blastic segmentation thresholds of $\mu-\sigma$ and $\mu+2\sigma$ were validated only for the CT scanning parameters stated above. Additional study is required to investigate whether different scanning parameters can resolve density differences between osteolytic structures and healthy trabecular bone more distinctly on CT images. Achieving this may necessitate a new definition of the lytic and blastic

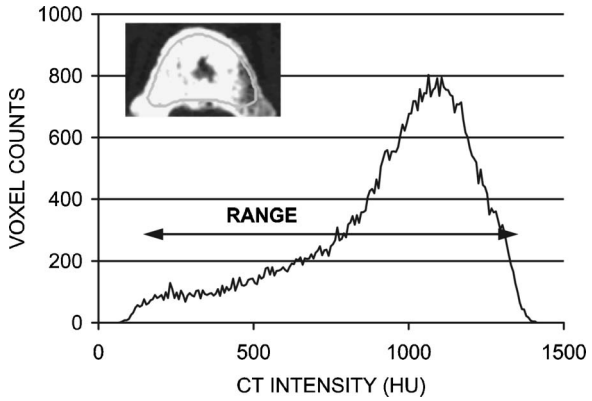

FIG. 5. Metastatic severity. Histogram range enables the severity of the metastatic disease to be quantified. A large range, stretching toward high-intensity voxels, is indicative of severe blastic involvement.

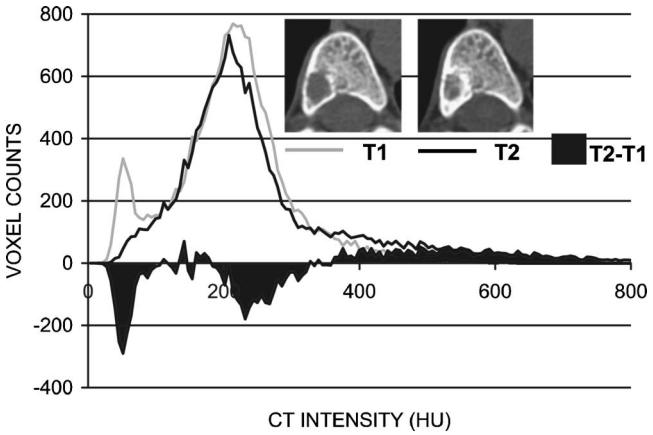

FIG. 6. Tumor progression. Histograms for the same vertebra from time periods T1 and T2 can be compared in order to quantify tumor progression. The difference is shaded between the two time points. Note the reduction in size of the lytic peak and increase in bright voxels correlating with the bony regrowth inside the tumor and surrounding area.

thresholds but may improve segmentation accuracy and precision. Furthermore, while the relationship between absolute range in CT numbers in a lesion and the extent of the disease has not been fully established, we have identified a relationship between blastic lesions and the larger than normal spread in CT numbers within the lesion itself. The significance of the range of CT numbers and tumor stage is a subject for future investigations.

The method for histogram analysis presented does provide a quantitative assessment of density distribution within the vertebral body; however, clinical interpretation is still crucial in verifying tumor involvement. The restoration of the Gaussian distributions of the healthy voxels was associated with the qualitative assessments of tumor involvement. However, it is important to note that CT intensity-based analysis does not distinguish between tumor-induced bone formation (blastic lesions), overcorrective healing, and calcifying treatment effects.

The assessment of tumor involvement utilizing this method also requires the presence of a healthy vertebral level. Patients in more advanced states of disease may have no vertebral levels unaffected by metastatic spread. As well, tumor involvement within the marrow space in some vertebrae may affect bone density measurements before any visible lytic or blastic lesions are evident on CT. Similarly, treatments that affect bone density, such as bisphosphonates, may affect both metastatically involved and healthy vertebral levels. The concurrent scanning of a standard qCT phantom with the acquisition of a spinal CT (e.g., RMI CT Phantom, Model 461, WI, USA) would help to normalize any density changes present in the healthy levels and account for intensity differences, which may occur due to scanning parameters in sequential scans.

The method is further limited in its ability to detect and track early metastatic involvement of vertebrae. The method is limited by the resolution of the images acquired in tracking distinct focal lesions. A reasonable limit is 3 or 4 voxels wide in plane, which in this study is 1.4 to 1.9 mm. For the quantification of diffuse tumors the detection limit will be determined by the changing distribution of CT numbers. The method should be quite sensitive to blastic diffuse disease because the threshold for blastic disease is two standard deviations above the mean, therefore little blastic tissue will overlap in intensity with normal tissue. To properly characterize the detection limit for lytic disease, which has similar CT numbers to those for marrow, a gold standard is needed to assess the detection limit. Future work in our laboratory will examine the relation of micro-CT imaging to histological sections in an animal study, which will provide a guide for determining the detection limit of the method for assessing lytic diffuse disease.

Previous clinical trials for new systemic therapeutic agents have often excluded patients with skeletal metastases from participating, due to the inability to quantify the effect of these treatments on the bony disease.[13] The quantitative assessments of disease progression and/or treatment effect in skeletal metastases may allow future studies to broaden inclusion criteria. This may permit patients most in need of novel therapeutics to realize their benefit during the research process.

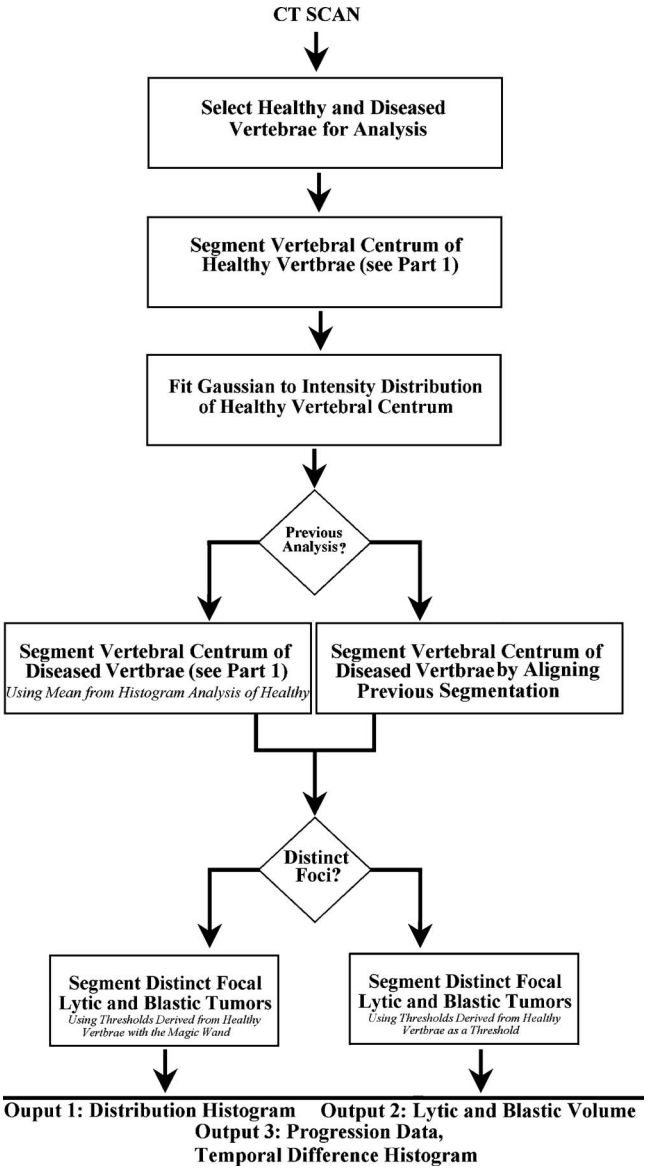

FIG. 7. Flow chart of proposed analysis for metastatically involved vertebrae. The segmentation of the vertebrae was the main subject of Part 1 of this work. This chart shows how the two parts are integrated into a single tool that can be used to quantify metastatic disease.

Skeletal related events (SREs) have been utilized as the standard measure in clinical trials for determining the effectiveness of new therapeutics aimed at skeletal metastases. The beneficial effects of newer therapeutics such as bisphosphonates have reduced the incidence of SREs. Thus, as new treatments for skeletal metastases are developed, clinical trials aimed at testing their effectiveness will require larger sample sizes in order to determine a significant impact due to the reduction in SRE incidence. Tracking the effects of new therapeutics on metastatically involved bone rather than focusing on SRE incidence may allow a reduction in the

sample size requirements in future clinical trials. Histogram analysis will also allow for effects of the therapeutics on healthy bones to be concurrently evaluated.

Our proposed histogram-based method for characterizing spinal metastases shows great potential in extending the quantitative capacity of CT-based radiographic evaluations. The development of a user-friendly tool for this purpose will encourage the tracking of metastatic progression and treatment effectiveness in clinical research applications (Fig. 7).

ACKNOWLEDGMENTS

Support for this study has been received from the Canadian Breast Cancer Research Alliance and the Natural Sciences and Engineering Research Council of Canada. Additional assistance on this project was also received from Angela Uzun, Geetha Metha, Basil Jardine, Patti Rainville, Edward Chow, Joel Rubenstein, Monique Christakis, and Albert Yee.

[a]Author to whom correspondence should be addressed. Electronic mail: cari.whyne@sunnybrook.ca

[1]D. A. Wong, V. L. Fornasier, and I. MacNab, "Spinal metastases: The obvious, the occult, and the impostors," Spine **15**, 1–4 (1990).
[2]R. D. Rubens, "Bone metastases—the clinical problem," Eur. J. Cancer **34**, 210–213 (1998).
[3]R. D. Roodman, "Biology of osteoclast activation in cancer," J. Clin. Oncol. **19**, 3562–3571 (2001).
[4]R. E. Coleman and R. D. Rubens, "The clinical course of bone metastases from breast cancer," Br. J. Cancer **55**, 61–66 (1987).
[5]G. N. Hortobagyi, R. L. Theriault, A. Lipton, L. Porter, D. Blayney, C. Sinoff, H. Wheeler, J. F. Simeone, J. J. Seaman, R. D. Knight, M. Heffernan, K. Mellars, and D. J. Reitsma, "Long-term prevention of skeletal complications of metastatic breast cancer with pamidronate: Protocol 19 Aredia Breast Cancer Study Group," J. Clin. Oncol. **16**, 2038–2044 (1998).
[6]R. L. Theriault, A. Lipton, G. N. Hortobagyi, R. Leff, S. Gluck, J. F. Stewart, S. Costello, I. Kennedy, J. Simeone, J. J. Seaman, R. D. Knight, K. Mellars, M. Heffernan, and D. J. Reitsma, "Pamidronate reduces skeletal morbidity in women with advanced breast cancer and lytic bone lesions: A randomized, placebo-controlled trial: Protocol 18 Aredia Breast Cancer Study Group," J. Clin. Oncol. **17**, 846–854 (1999).
[7]R. E. Coleman, "Management of bone metastases," Oncologist **5**, 463–470 (2000).
[8]P. LoRusso, "Analysis of skeletal-related events in breast cancer and response to therapy," Semin. Oncol. **28**, 22–27 (2001).
[9]N. Janjan, "Bone metastases: Approaches to management," Semin. Oncol. **28**, 28–34 (2001).
[10]J. L. Hayward, P. P. Carbone, J. C. Heusen, S. Kumaoka, A. Segaloff, and R. D. Rubens, "Assessment of response to therapy in advanced breast cancer," Br. J. Cancer **35**, 292–298 (1977).
[11]J. L. Hayward, P. P. Carbone, R. D. Rubens, J. C. Heuson, S. Kumaoka, and A. Segaloff, "Assessment of response to therapy in advanced breast cancer (an amendment)," Br. J. Cancer **38**, 201 (1978).
[12]WHO Handbook for Reporting Results of Cancer Treatment, Geneva (Switzerland), World Health Organization Offset Publication (1979).
[13]T. Hamaoka, J. E. Madewell, D. A. Podoloff, G. N. Hortobagyi, and N. T. Ueno, "Bone imaging in metastatic breast cancer," J. Clin. Oncol. **22**, 2942–2953 (2004).
[14]P. Therasse, S. G. Arbuck, E. A. Eisenhauer, J. Wanders, R. S. Kaplan, L. Rubinstein, J. Verweij, M. Van Glabbeke, A. T. van Oosterom, M. C. Christian, and S. G. Gwyther, "New guidelines to evaluate the response to treatment in solid tumors: European Organization for Research and Treatment of Cancer, National Cancer Institute of the United States, National Cancer Institute of Canada," J. Natl. Cancer Inst. **92**, 205–216 (2000).
[15]C. S. Galasko, "Skeletal metastases and mammary cancer," Ann. R. Coll. Surg. Engl. **50**, 3–28 (1972).
[16]J. Vinholes, R. Coleman, and R. Eastell, "Effects of bone metastases on bone metabolism: Implications for diagnosis, imaging and assessment of response to cancer treatment," Cancer Treat Rev. **22**, 289–331 (1996).
[17]L. D. Rybak and D. I. Rosenthal, "Radiological imaging for the diagnosis of bone metastases," Q. J. Nucl. Med. **45**, 53–64 (2001).
[18]G. A. Edelstyn, P. J. Gillespie, and F. S. Grebbell, "The radiological demonstration of osseous metastases: Experimental observations," Clin. Radiol. **18**, 158–162 (1967).
[19]G. N. Hortobagyi, H. I. Libshitz, and J. E. Seabold, "Osseous metastases of breast cancer. Clinical, biochemical, radiographic, and scintigraphic evaluation of response to therapy," Cancer **53**, 577–582 (1984).
[20]C. S. Galasko, "The value of scintigraphy in malignant disease," Cancer Treat Rev. **2**, 225–272 (1975).
[21]R. E. O'Mara, "Skeletal scanning in neoplastic disease," Cancer **37**, 480–486 (1976).
[22]J. Muindi, R. C. Coombes, S. Golding, T. J. Powles, O. Khan, and J. Husband, "The role of computed tomography in the detection of bone metastases in breast cancer patients," Br. J. Radiol. **56**, 233–236 (1983).
[23]R. J. Corcoran, J. H. Thrall, R. W. Kyle, R. J. Kaminski, and M. C. Johnson, "Solitary abnormalities in bone scans of patients with extraosseous malignancies," Radiology **121**, 663–667 (1976).
[24]M. Tubiana-Hulin, "Incidence, prevalence, and distribution of bone metastases," Bone (N.Y.) **12**, S9–S10 (Suppl. 1) (1991).
[25]T. G. Sanders and T. W. Parsons, "Radiographic imaging of musculoskeletal neoplasia," Cancer Control **8**, 221–231 (2001).
[26]D. L. Citrin, R. G. Bessent, and W. R. Greig, "A comparison of the sensitivity and accuracy of the 99TCm-phosphate bone scan and skeletal radiograph in the diagnosis of bone metastases," Clin. Radiol. **28**, 107–117 (1977).
[27]C. S. Galasko and F. H. Doyle, "The detection of skeletal metastases from mammary cancer: A regional comparison between radiology and scintigraphy," Clin. Radiol. **23**, 295–297 (1972).
[28]Y. T. Lee, "Bone scanning in patients with early breast carcinoma: Should it be a routine staging procedure?" Cancer **47**, 486–495 (1981).
[29]R. E. Coleman, R. D. Rubens, and I. Fogelman, "Reappraisal of the baseline bone scan in breast cancer," J. Nucl. Med. **29**, 1045–1049 (1988).
[30]D. D. Dershaw and M. Osborne, "Imaging techniques in breast cancer," Semin Surg. Oncol. **5**, 82–93 (1989).
[31]G. J. Cook and I. Fogelman, "The role of positron emission tomography in the management of bone metastases," Cancer **88**, 2927–2933 (2000).
[32]B. R. Condon, R. Buchanan, N. W. Garvie, D. M. Ackery, J. Fleming, D. Taylor, D. Hawkes, and B. A. Goddard, "Assessment of progression of secondary bone lesions following cancer of the breast or prostate using serial radionuclide imaging," Br. J. Radiol. **54**, 18–23 (1981).
[33]R. H. Daffner, A. R. Lupetin, N. Dash, Z. L. Deeb, R. J. Sefczek, and R. L. Schapiro, "MRI in the detection of malignant infiltration of bone marrow," AJR, Am. J. Roentgenol. **146**, 353–358 (1986).
[34]D. K. Kido, R. Gould, F. Taati, A. Duncan, and J. Schnur, "Comparative sensitivity of CT scans, radiographs, and radionuclide bone scans in detecting metastatic calvarial lesions," Radiology **128**, 371–375 (1978).
[35]R. E. Coleman, "Monitoring of bone metastases," Eur. J. Cancer **34**, 252–259 (1998).
[36]M. Sundaram and M. H. McGuire, "Computed tomography or magnetic resonance for evaluating the solitary tumor or tumor-like lesion of bone?," Skeletal Radiol. **17**, 393–401 (1988).
[37]E. Chow, L. Holden, J. Rubenstein, M. Christakis, K. Sixel, M. Vidmar, J. Finkelstein, C. Hayter, A. Loblaw, R. Wong, E. Szumacher, and C. Danjoux, "Computed tomography (CT) evaluation of breast cancer patients with osteolytic bone metastases undergoing palliative radiotherapy–a feasibility study," Radiother. Oncol. **70**, 291–294 (2004).
[38]K. T. Bae, P. Fuangtharnthip, S. R. Prasad, B. N. Joe, and J. P. Heiken, "Adrenal masses: CT characterization with histogram analysis method," Radiology **228**, 735–742 (2003).
[39]H. Nomori, T. Ohtsuka, T. Naruke, and K. Suemasu, "Histogram analysis of computed tomography numbers of clinical T1 N0 M0 lungadenocarcinoma, with special reference to lymph node metastasis and tumor invasiveness," J. Thorac. Cardiovasc. Surg. **126**, 1584–1589 (2003).
[40]C. Whyne, L. Gordon, M. Hardisty, P. Agarwal, and T. Skrinskas, "Automated segmentation of the metastatic spine using atlas-based deformable registration and the level set method," Med. Phys. **34**, 3127–3134 (2007).